A linear MPC approach for longitudinal stability of hydrofoiling AC45 catamarans

Joshua Amato (4688368), Tom de Jonge (4905350)

***Abstract*—We study a linear model predictive control (MPC) approach for the longitudinal stability of AC45 hydrofoiling catamarans under disturbed conditions. A state-feedback- and output-feedback based controller are designed and compared to LQR through numerical simulations. The stability of the state-feedback controller is proved analytically for an ellipsoid terminal set. It is shown that the MPC succeeds in stabilizing the states on a constant reference, even under disturbed conditions.**

I. Introduction

A. Hydrofoiling Catamarans

Hydrofoiling, often employed in sailboat racing, involves the use of a lifting surface called a foil beneath the boat's hull. As the vessel moves forward through the water, this hydrofoil generates lift, elevating the hull above the waterline. This reduces the contact area between the boat and the water, enabling the boat to reach significantly greater speeds [1].

The most prominent example of a sailing boat utilizing hydrofoils to great effect is the AC45 catamaran, a high-performance racing vessel used in the America's Cup World Series. Although hydrofoils can greatly increase the velocity of boats, they also come with some added complexities. Foiling vessels are sensitive to changes in pitch and roll, as almost all stability is lost due to the minimal hull contact with the water. Therefore, the sailors were posed with the challenge of learning to control the foils in such a way that the dynamics of the vessel remained stable while maintaining as much speed as possible.

In the early days of foiling, technology was not advanced enough to accurately simulate the behaviour of these foiling vessels. Therefore, the teams used physical models and experiments to gather data about the dynamics of the vessels. However, as time progressed and simulation technology improved, it has become possible to use modeling techniques and control theory to design effective controllers, capable of stabilizing the boats while allowing for maximum velocity.

These systems can be employed to regulate control inputs, such as flaps on the hydrofoils and rudder. The controller constantly tweaks the position of these control surfaces in order to track target references for ride height and pitch angle. This means the boat's stability during varying conditions, such as changes in boat speed, wind speed, current or waves, can be maintained.

Joshua Amato and Tom de Jonge are master students at TU Delft, The Netherlands. E-mail addresses: {j.amato, t.j.dejonge}@student.tudelft.nl.

B. Research Goal and Contributions

For this project, the goal is to create a model predictive control system capable of coordinating the daggerboard and rudder foil angles in such a way that the boat ride height tracks a constant reference height and the pitch angle is stabilized. Improvement in performance can be vital for racing teams to better understand how to optimally control their vessels under changing circumstances. Although the direct use of these systems is prohibited during racing [2], the technology is still valuable to teams, as it provides reference for the crew on board to follow and can provide information on what types of maneuvers are the most effective [3]. Moreover, MPC controller development benefits applications beyond racing, such as stabilizing foiling ferries for smoother rides and reduced passenger discomfort.

The MPC reference tracking and output feedback designs created in this project are compared with the design of the LQR by Bencatel et al. [4]. In addition, Luenberger observers are used in the present work in contrast to the Kalman filter of [4]. This paper is structured as follows. First, the nonlinear and linearized models that have been used to predict the dynamics of the AC45, obtained from [4], are explained. Secondly, we discretize their model and extend it to include constant and Gaussian additive disturbances. Subsequently, the linear MPC is formulated and asymptotic stability is proven. Lastly, numerical simulations under various conditions show the performance of our design.

C. Notation

The spectrum of a matrix $A \in \mathbb{R}^{n\times n}$ is noted by spec(A) and its eigenvalues $\lambda_{i=1,\dots,n} \in$ spec(A). In addition, the observability and controllability matrix of pairs (A, C) and (A, B) are denoted by $\mathcal{O}(A, C)$ and $\mathcal{C}(A, B)$ respectively. Call the open unit disc $\mathbb{D}_0 = \{c \in \mathbb{C} |\, |c| < 1\}$. The singular values of some matrix M are noted by $\Sigma = diag(\sigma_{max,M}, \dots, \sigma_{min,M})$. A diagonal matrix $D \in \mathbb{R}^{n\times n}$ with scalars $a_{i=1,\dots,n}$ is denoted as $diag(a_1, \dots, a_n)$. A block diagonal matrix $B \in \mathbb{R}^{Mn\times Mm}$ with entries $W_{i=1,\dots,M} \in \mathbb{R}^{n\times m}$ is denoted as $blkdiag(W_1, \dots, W_M)$. $\mathbf{u}_N = (u(0), u(1), \dots, u(N-1)) \in \mathbb{R}^{n_u\times N}$ denotes an input sequence, where $u \in \mathbb{R}^{n_u}$ denotes the system input. An equivalent notation is used for the state: $\mathbf{x}_N = (x(0), x(1), \dots, x(N-1)) \in \mathbb{R}^{n_x\times N}$. The asterisk in a vector $\begin{bmatrix} 0 & * & * \end{bmatrix}$ indicate the continuation of the element on the left. Lastly, denote $\mathbf{v_1} = \begin{bmatrix} 1 & -1 \end{bmatrix}^T$, $\mathbf{1}_N$ and $\mathbf{0}_N$ as N dimensional vectors of ones and zeros respectively, whilst $\mathbf{1}_{N\times M}$ and $\mathbf{0}_{N\times M}$ as $N \times M$ matrices of ones and zeros.

D. System Dynamics

The system dynamics are described by a linearized 3 degree of freedom (DOF) model that is derived from [4] which is similar to the model described in [5]. In this paper, R. Bencatel et al. [4] used a 6-DOF model and designed a full state feedback controller using LQR theory to compute the gains. Furthermore, they linearized the model at a speed of 21.7 knots to derive a simpler 3-DOF model that only considers the longitudinal dynamics, including horizontal speed, height, and pitch. The parameters were obtained directly from a velocity prediction program of the AC45 Luna Rossa test yachts. This parameterized model is used for the controller design in the present work.

The nonlinear time-invariant equations used to describe the AC45's longitudinal dynamics (in continuous time) are shown below. Ship-related terminology is clarified in figure 1. The state vector considered is given by $x := \begin{bmatrix} V_H & \gamma & q & z & \theta \end{bmatrix}^T$ where V_H is the boat's hydrodynamic speed, γ is the flight path angle, q is the boat's angular velocity in the pitch direction, z is the ride height, and θ is the pitch angle. Furthermore, the control inputs are the daggerboard and rudder rake angles δ_{Rake} and δ_e, yielding $u := \begin{bmatrix} \delta_{Rake} & \delta_e \end{bmatrix}^T$. The dynamics are then given by:

$$f(x,u) = \begin{pmatrix} \frac{1}{m}(F_{w_x} - mg\sin(\gamma) - D) - V_H q(\theta - \gamma) \\ \\ \frac{1}{mV_H}(L - mg\cos(\gamma)) \\ \\ \frac{1}{I_{yy,HC}}(\mathcal{M} + z_{WAC,HC}F_{W_x} \\ + mg(x_{CM,HC}\cos(\theta) + z_{CM.HC}\sin(\theta)) \\ \\ V_H\gamma \\ \\ q\cos(\phi) - r\sin(\phi) \end{pmatrix} \tag{1}$$

The variables in equation 1 that are not state variables are described in the table below. Note that CM refers to the center of mass and HC refers to the hydrodynamic center.

Variable	Description
F_{w_x}	Wind force projected on $\mathbf{x}_w$ (see fig 1)
D	boat Drag force
m	boat mass
L	boat lift force
$I_{yy,HC}$	moment of inertia at HC
$z_{WAC,HC}$	height of wing aerodynamic center with respect to HC
$x_{CM,HC}$	Distance in the x direction of CM from HC
$z_{CM,HC}$	height of CM from HC
ϕ	roll angle (heel) of boat

TABLE I
DESCRIPTION OF VARIABLES NOT INCLUDED IN THE STATE-VECTOR FROM EQUATION 1

It must be noted that in this model it is assumed the catamaran has negligible heel. More formally: $\phi \approx 0$ and therefore: $\dot{\theta} \approx q$. Furthermore, the careful reader might have noted that the elements of u are not explicitly stated in $f(x,u)$. These are implicit in the pitching movement $\mathcal{M}$ since:

$$\begin{aligned} \mathcal{M} &= \frac{\rho V_H^2}{2} S c C_m \\ C_m &= C_{m0} + \frac{\partial C_m}{\partial V_H}V_H + \frac{\partial C_m}{\partial \alpha}\alpha\frac{\partial C_m}{\partial z_{foil}}z_{foil} \\ &\quad + \frac{\partial C_m}{\partial \dot{\alpha}}\dot{\alpha} + \frac{\partial C_m}{\partial \beta}\beta + \frac{\partial C_m}{\partial \phi}\phi + \frac{\partial C_m}{\partial \delta_{Rake}}\delta_{Rake}\frac{\partial C_m}{\partial \delta_e}\delta_e \end{aligned} \tag{2}$$

where z_{foil} is the depth to which the foil is submerged, S is the foil reference area and c is the foil reference mean chord. C_m describes the dynamics of the center of mass.

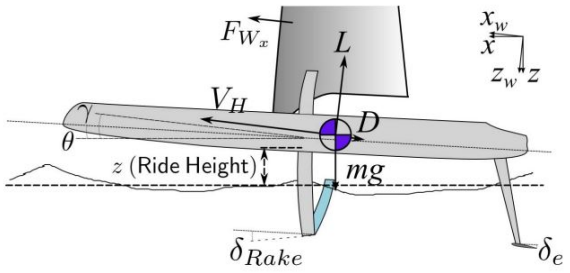

Fig. 1. Longitudinal Force Diagram. Adapted from [4].

E. Linear System Dynamics

The nonlinear system can be linearized using the general formula:

$$A = \left.\frac{\partial f(x,u)}{\partial \bar{x}}\right|_{(\bar{x},0)},\ B = \left.\frac{\partial f(x,u)}{\partial u}\right|_{(\bar{x},0)}$$
$$C = \left.\frac{\partial h(x,u)}{\partial \bar{x}}\right|_{(\bar{x},0)},\ D = \left.\frac{\partial h(x,u)}{\partial u}\right|_{(\bar{x},0)}$$

.

$h(x,u)$ is a (nonlinear) output map $(x,u) \mapsto (z,\theta)$. The linearized continuous-time system is then given by:

$$\begin{cases} \dot{x} = Ax + Bu, \quad x(0) = x_0 \\ y = Cx + Du \end{cases} \tag{3}$$

The derivation of the linearized system is not explicitly described here since it is outside of the scope of this project and the parameterized linearization on which we base our work is already provided in [4].

The first extension to [4] is the discretization of equation 3 using zero-order hold. This discretization method is chosen because it is the most simple to implement in a real-world setting. The discrete-time state equation becomes:

$$\begin{aligned} x(k+1) &= e^{Ah}x(k) + \int_0^h e^{As}B\,ds\ u(k) \\ &= \Psi x(k) + \Gamma u(k) \end{aligned} \tag{4}$$

where $k \in \mathcal{T} \subseteq \mathbb{N}$ is the sample number and h is the inter-sampling time in seconds. In the MPC framework this is conveniently noted as:

$$\begin{aligned} x^+ &= \Psi x + \Gamma u \\ y &= Cx + Du \end{aligned} \tag{5}$$

where the superscript $^+$ indicates the next sampling instant. The inter-sampling time has been chosen as $h = 0.5\ s$, slightly higher than in the work of [4] ($h = 0.1\ s$) since we noticed numerical issues in the optimization when discretizing at this rate. It is superfluous to state the numerical values of the state matrices; however, it is important to mention that the output is given by:

$$y = Cx = \begin{bmatrix} 0 & 0 & 0 & 1 & 0 \\ 0 & 0 & 0 & 0 & 1 \end{bmatrix} x, \qquad (D = 0) \tag{6}$$

F. Linear System Dynamics with Additive Disturbances

The discrete-time system is augmented with constant disturbance $d \in \mathbb{R}^{n_y}$ and discrete-time Gaussian white noise, representing non-modelled effects such as wind gusts, waves or sensor errors. The latter is an independent sequence $v : \Omega \times \mathcal{T} \to \mathbb{R}^{n_y}$ defined on a measurable space (Ω, F) such that $v \in G(0, I_{n_y}) \quad \forall k \in \mathcal{T}$ where $G(0, Q_v)$ is a Gaussian distribution with variance Q_v (def. 3.4.1 in [6]). The noise process $w \in \mathbb{R}^{n_x}, w \in G(0, I_{n_x})$ is defined analogously. The augmented system becomes:

$$\begin{aligned} x^+ &= \Psi x + \Gamma u + \Gamma_d d + Mw \\ y &= Cx + C_d d + Nv \end{aligned} \tag{7}$$

where $\Gamma_d \in \mathbb{R}^{n_x \times n_d}$, $C_d \in \mathbb{R}^{n_y \times n_d}$, $M \in \mathbb{R}^{n_x \times n_w}$, and $N \in \mathbb{R}^{n_y \times n_v}$ are deterministic and known. These are chosen as:

$$\begin{aligned} &\Gamma_d = \begin{bmatrix} 1 & 0 \\ 0.5 & 1 \\ \mathbf{0}_3 & \mathbf{0}_3 \end{bmatrix}, \quad C_d = \begin{bmatrix} 1 & 0 \\ 0.5 & 0 \end{bmatrix} \\ &M = sI_{n_x}, \quad N = sI_{n_y} \end{aligned} \tag{8}$$

where $s = 0.005$ and $d = \begin{bmatrix} 0.03 & 0.01 \end{bmatrix}^T$. This means we have a relatively large disturbance on the hydrodynamic speed and flight path angle. The disturbance on the ride height and pitch angle is about 10% of the reference height and overshoot respectively using state feedback without disturbances (see section IV-B).

II. Model predictive control design

In this section, we show that the designed MPC asymptotically stabilizes the closed-loop system. With this aim, we verify the assumptions of Theorem 2.24 in the book [7]. However, we first show additional results that are necessary for the verification of the assumptions.

A. Controllability and Observability

Firstly, let us consider the system stated in equations 5, by `rank()` in MATLAB for $\Psi \in \mathbb{R}^{n_x \times n_x}$:

$$\begin{aligned} &\text{rank}(\mathcal{C}(\Psi, \Gamma)) = n_x \\ &\text{rank}(\mathcal{O}(\Psi, C)) = n_x \end{aligned} \tag{9}$$

To avoid false conclusions originating from numerical errors, we compute the singular value decomposition of both $\mathcal{C}(\Psi, \Gamma)$ and $\mathcal{O}(\Psi, C)$. This shows that, respectively, $\sigma_{min,\mathcal{C}} = 0.2622$ and $\sigma_{min,\mathcal{O}} = 0.0438$ which was deemed reasonable to conclude non-singularity. Therefore, we conclude that (Ψ, Γ) is a controllable pair and that (Ψ, C) is an observable pair. Lastly, $\text{spec}(\Psi) \not\subset \mathbb{D}_0$ since for $\lambda_{i=1,\dots,5} \in \text{spec}(\Psi)$, $\lambda_5 = 1.0282$. Hence, the origin is locally unstable.

For the augmented system, it is necessary to check an auxiliary condition. We have verified that:

$$\text{rank}(\begin{bmatrix} I - A & -\Gamma_d \\ C & C_d \end{bmatrix}) = n_x + n_d \tag{10}$$

including the same verification on the singular values. Hence, since (Ψ, C) observable we can conclude that the augmented system is observable (see Lemma 1 of Pannocchia and Rawlings [8]).

B. Constraints

The input constraints are motivated by a hydrodynamic consideration. It is imperative to avoid stalling due to the angle of the daggerboard foil. This can be done by limiting its angle of attack β. Although the literature on the foils of this specific type of catamaran is fairly limited, we concluded that stall can occur from $\beta \in [12°, 15°]$ [9], [10]. As a safety limit we employ a bound: $\bar{\beta} = 12°$. Assuming the velocity $V_{water} \parallel V_H$, it can be seen that $\beta = \gamma - \theta + \delta_{Rake}$. Therefore, the constraint can be formulated as: $|\delta_{Rake} + \gamma - \theta| \leq \bar{\beta}$. The rudder angle is simply bounded to minimize drag: $|\delta_e| \leq \bar{\delta_e}$. The bound $\bar{\delta_e}$ is deducted from the results in [4], and set to: $\bar{\delta_e} = 5°$. The input constraints can be written compactly as (see section I-C for notation):

$$\begin{aligned} &F_1 x + E_1 u \leq e_1, \quad e_1 = \begin{bmatrix} \bar{\beta} & \bar{\beta} & \bar{\delta_e} & \bar{\delta_e} \end{bmatrix}^T \\ &F_1 = \begin{bmatrix} \mathbf{0_2} & \mathbf{v_1} & \mathbf{0_2} & \mathbf{0_2} & \mathbf{v_1} \\ \mathbf{0_2} & * & * & * & * \end{bmatrix}, \; E_1 = blkdiag(\mathbf{v_1}, \mathbf{v_1}) \end{aligned} \tag{11}$$

Tight state constraints are implemented only on the the ride height z. By observing the experimental and numerical results in [4], a maximum allowed deviation of 0.5 meters upwards and 0.315 meters downwards has been determined:

$$\begin{aligned} &F_2 x \leq e_2 \\ &F_2 = \begin{bmatrix} \mathbf{0_2} & * & * & \mathbf{v_1} & \mathbf{0_2} \end{bmatrix}, \; e_2 = \begin{bmatrix} 0.5 \\ 0.315 \end{bmatrix} \end{aligned} \tag{12}$$

To obtain a closed and compact set $\mathbb{X}$ (see eq. 15) we impose the following loose constraints on the remaining state variables.

$$\begin{aligned} &F_3 x \leq e_3, \\ &F_3 = \begin{bmatrix} \mathbf{v_1} & \mathbf{0_2} & * & * & * \\ \mathbf{0_2} & \mathbf{v_1} & \mathbf{0_2} & * & * \\ \mathbf{0_2} & \mathbf{0_2} & \mathbf{v_1} & \mathbf{0_2} & * \\ \mathbf{0_2} & * & * & * & \mathbf{v_1} \end{bmatrix}, \; e_3 = \begin{bmatrix} 5 \cdot \mathbf{1_2} \\ 20° \cdot \mathbf{1_2} \\ 20° \cdot \mathbf{1_2} \\ 20° \cdot \mathbf{1_2} \end{bmatrix} \end{aligned} \tag{13}$$

The final constraint equation can therefore be denoted as:

$$\begin{bmatrix} F_1 \\ F_2 \\ F_3 \end{bmatrix} x + \begin{bmatrix} E_1 \\ \mathbf{0}_{4\times 2} \\ \mathbf{0}_{8\times 2} \end{bmatrix} u \leq \begin{bmatrix} e_1 \\ e_2 \\ e_3 \end{bmatrix} \\ \mathbf{F}x + \mathbf{E}u \leq \mathbf{e} \quad \forall k \in \mathcal{T} \tag{14}$$

We can now define the euclidean spaces:

$$(\mathbb{X}, \mathbb{U}) := (\{(x \in \mathbb{R}^5, u \in \mathbb{R}^2) \mid \mathbf{F}x + \mathbf{E}u \leq \mathbf{e}\} \\ \mathbb{Z} := \mathbb{X} \times \mathbb{U} \tag{15}$$

C. State-Feedback MPC

We consider a receding horizon MPC strategy with control horizon $N = 20$ and quadratic stage cost function $\ell(x(k), u(k)) = \frac{1}{2}x(k)^T Q x(k) + \frac{1}{2}u(k)^T R u(k)$ where the matrices $Q = diag(0.1, 10, 1, 100, 1)$ and $R = diag(1, 0.1)$. The weights have been chosen to reflect the relative importance of the state variables. That is, we want to penalize deviations of z and θ the most in that order, followed by variables by which they are influenced. The matrix R has been chosen as such since we would like to use the rudder more than in reference [4], as we conjecture that this reduces hydrodynamic drag. The terminal cost function is chosen as $V_{\mathrm{f}}(x(N)) = \frac{1}{2}x(N)^T P x(N)$ with the elliptic terminal set $\mathbb{X}_{\mathrm{f}} = \{x \in \mathbb{R}^{n_x} \mid V_f(x) \leq 1\}$ where P solves the discrete-time algebraic Riccati equation (DARE):

$$A_K^T P A_K - P = -Q_K, \quad P \succ 0 \\ A_K = \Psi + \Gamma K, \quad Q_K = Q + K^T R K \\ K = -(\Gamma^T P \Gamma + R)^{-1} \Gamma^T P \Psi^T \tag{16}$$

Hence, the cost function becomes:

$$V_N(x, \mathbf{u}_N) = \frac{1}{2}\sum_{k=0}^{N-1} \{x(k)^T Q x(k) + u(k)^T R u(k)\} \\ + \frac{1}{2}x(N)^T P x(N) \tag{17}$$

with the optimal input sequence $\mathbf{u}_N^0 = \operatorname{argmin}_{\mathbf{u}_N} V_N(x, \mathbf{u}_N)$. The (parameteric) optimal control problem $\mathbb{P}_N(x_0, t)$ is then defined as a quadratically constrained quadratic porgram (QCQP):

$$\mathbb{P}_N(x_0) := \begin{cases} \min\limits_{u_N} & V_N(x_0, \mathbf{u}_N) \\ \text{s.t.} & x^+ = \Psi x + \Gamma u \quad \forall k \\ & \mathbf{F}x + \mathbf{E}u \leq \mathbf{e} \quad \forall k \\ & x(N) \in \mathbb{X}_f \\ & x(0) = x_0 \end{cases} \tag{18}$$

Note that in this framework $x(0) = x(k)$.

D. Output-Feedback Reference-Tracking MPC

As shown in section II-A, the augmented system is observable. Therefore we can reconstruct the full state vector using Luenberger observers. Here, one estimates the constant disturbance and corrects the state estimate accordingly. Let $\hat{x}$ and $\hat{d}$ be the estimated state and disturbance, respectively. In addition, let $\tilde{L} = \begin{bmatrix} L_1^T & L_2^T \end{bmatrix}^T$ be the observer gain partitioned in a part for the state and a part for the disturbance. The estimated state evolution is described by:

$$\begin{bmatrix} \hat{x}^+ \\ \hat{d}^+ \end{bmatrix} = \underbrace{\begin{bmatrix} A & B_d \\ 0 & I \end{bmatrix}}_{\tilde{A}} \begin{bmatrix} \hat{x} \\ \hat{d} \end{bmatrix} + \begin{bmatrix} B \\ 0 \end{bmatrix} u + \underbrace{\begin{bmatrix} L_1 \\ L_2 \end{bmatrix}}_{\tilde{L}} (y - \underbrace{\begin{bmatrix} C & C_d \end{bmatrix}}_{\tilde{C}} \begin{bmatrix} \hat{x} \\ \hat{d} \end{bmatrix}) \tag{19}$$

where we choose $\tilde{L}$ such that $\mathrm{spec}(\tilde{A} - \tilde{L}\tilde{C}) \subset \mathbb{D}_0$, in our design $\mathrm{spec}(\tilde{A} - \tilde{L}\tilde{C}) \in [0.3, 0.4]$.

In order to track a reference, it is necessary to shift the terminal set around the reference state vector. That is $\mathbb{X}_f' = \{x_{ref}\} \oplus \mathbb{X}_f \subseteq \mathbb{X}$. The shifted terminal set is defined as $\mathbb{X}_f' := \{x \in \mathbb{R}^{n_x} \mid (x - x_{ref})^T P (x - x_{ref}) \leq 1\}$. In addition, it is necessary to reformulate the quadratic stage cost function as $\ell'(x(k), u(k)) = \frac{1}{2}(x(k) - x_{ref})^T Q (x(k) - x_{ref}) + \frac{1}{2}(u(k) - u_{ref})^T R (u(k) - u_{ref})$, where the weight matrices are the same as before, and the terminal cost $V_f'(x(N) = (x(N) - x_{ref})^T P (x(N) - x_{ref})$. The reference input u_{ref} and state x_{ref} are obtained by solving an online *optimal target selection* (OTS) problem, formulated as:

$$\begin{aligned} \underset{x_{ref}, u_{ref}}{\text{argmin}} \quad & ||u_{ref}||_2 \\ \text{s.t.} \quad & \begin{bmatrix} I - A & -B \\ C & 0 \end{bmatrix} \begin{bmatrix} x_r \\ u_r \end{bmatrix} = \begin{bmatrix} B_d \hat{d} \\ y_{ref} - C_d \hat{d} \end{bmatrix}, \\ & (x_{ref}, u_{ref}) \in \mathbb{Z}, \\ & C x_r + \hat{d} \in \mathbb{Y} \end{aligned} \tag{20}$$

where $\mathbb{Y}$ is the corresponding constrained output space. In conclusion, the optimal control problem has an equivalent formulation as 18, albeit with the newly defined ingredients.

III. Asymptotic stability

A. On the terminal set

First, we describe the procedure to show numerically that assumption 1 on the terminal set $\mathbb{X}_{\mathrm{f}}$ is valid. In addition, Lemma 1 shows, positive invariance of the terminal set for the design we employed under the MPC control law. The result is used in the following subsection to ensure that assumption 2.14 of [7] holds. Here, we introduce the MPC control law $\kappa : \mathbb{X} \times \mathcal{T} \to \mathbb{U}$ such that $u(t) = \kappa(t, x(t))$.

Assumption 1: Let the terminal cost $V_f(x) = \frac{1}{2}x^T P x$ for some $P > 0$ and the terminal set $\mathbb{X}_{\mathrm{f}} = \{x \in \mathbb{R}^{n_x} \mid V_f(x) \leq c\}$ such that $c > 0$. Then (a) $\mathbb{X}_f \subseteq \mathbb{X}$ and for feedback gain K (b) $Kx \in \mathbb{U}\ \forall x \in \mathbb{X}_f$.

Procedure 1: The general idea is to come up with a polytopic outer approximation of the ellipsoid terminal set and to check that the conditions of the approximation are satisfied. Since for our design we have $P = P^T$ the diagonalization $P = U \Lambda U^T$ is orthogonal. That is, U is an orthogonal eigenvector basis. Herein is $\Lambda = diag(\lambda_1, \ldots, \lambda_5)$. By substitution we have that $x^T P x \leq c$ can be written as $x^T U \Lambda U^T x \leq c$. If we make the substitution $y = U^T x$ then $y^T \Lambda y \leq c$, which can be conveniently rewritten as $\sum_{i=1}^5 \lambda_i y_i^2 \leq c$ where

y_i is the i-th entry of y. Now we can make the important observation that due to orthogonality of U, $y^T\Lambda y = c$ implies $y_i = \pm\sqrt{\frac{c}{\lambda_i}}$. That is, each eigenvector i intersects the ellipsoid at these points which are the outer points of the ellipsoid semi-axes. To check whether the ellipsoid is in the respective sets, we define an outer approximation $\mathcal{P}_{out}(\mathcal{V}) \supset \mathbb{X}_f$ with vertices $\mathcal{V}$, which is a higher dimensional rhombus with $\mathcal{V} := \{U\bar{y}_1, U\bar{y}_2, \dots, U\bar{y}_5, -U\bar{y}_1, -U\bar{y}_2, \dots, -U\bar{y}_5\}$. Here, $\bar{y}$ is the vector with its i-th entry $\bar{y}_i = 2\sqrt{\frac{c}{\lambda_i}}$.

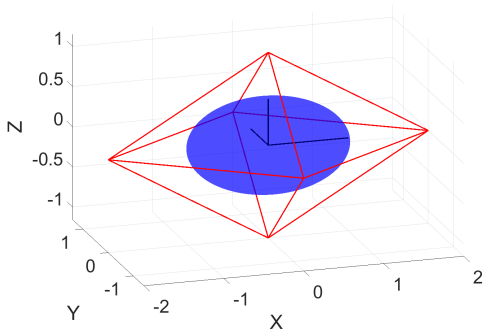

Fig. 2. Illustration of hyperrhombus (red) approximating an ellipsoid (blue) with its vertices along the ellipsoids' semi axes (black)

Since all elements in the convex set are linear combinations of its vertices it can be seen that we can check all elements of $\mathcal{V}$ such that $\forall x \in \mathcal{P}_{out}$ the set inequalities hold. Furthermore, since $\mathcal{P}_{out}(\mathcal{V}) \supset \mathbb{X}_f$, $\mathcal{P}_{out}(\mathcal{V}) \subseteq \mathbb{X}$ implies $\mathbb{X}_f \subset \mathbb{X}$ and if $Kx \in \mathbb{U}\ \forall x \in \mathcal{P}_{out}(\mathcal{V})$ then $Kx \in \mathbb{U}\ \forall x \in \mathbb{X}_f$. By coordinate transformation, we may conveniently check this by choosing c such that:

$$\mathbf{F}U\bar{y} + \mathbf{E}KU\bar{y} \leq \mathbf{e}$$

where K comes from the DARE solution. Using an iterative procedure in MATLAB, we have reached $c = 1$. Equivalently, for the set $\mathbb{X}_f'$ we can employ the same procedure.

Lemma 1: Assume that $V_f(x) = \frac{1}{2}x^TPx$, $\mathbb{X}_\mathrm{f} = \{x \in \mathbb{R}^{n_x} |\ V_f(x) \leq c\}$ such that $c > 0$, where $P > 0$ $P = P^T$ solves the DARE in equation 16. Furthermore, assume that $V_f(A_Kx) \leq V_f(x) - \frac{1}{2}l(x,u)$ with K defined in equation 16, that assumption 1 holds and that assumption 2.2, 2.3, and 2.14(b) hold of [7]. Then $\mathbb{X}_f$ is positive invariant for $x^+ = Ax + B\kappa_N(x)$.

Proof: Observe that due to the assumption $V_f(A_Kx) \leq V_f(x) - \frac{1}{2}l(x,u)$, $\mathbb{X}_\mathrm{f} = \{x \in \mathbb{R}^{n_x} \mid V_f(x) \leq c\}$ is positive invariant by construction for $x^+ = A_Kx$. Furthermore, note that $V_f = \frac{1}{2}x^TPx = V_\infty^{uc}(x)$ where $V_\infty^{uc}(x)$ is the optimal infinite-horizon value function. By the Bellman optimality principle we have that within $\mathbb{X}_f$:

$$V_N^{uc} = \min_{\mathbf{u}_N} V_N(x, \mathbf{u}_N) = V_\infty^{uc}(x) = V_f(x)$$

Subsequently, we restrict the terminal set by assuming $\mathcal{X}_n \supseteq \mathbb{X}_f$, thus reducing the freedom of optimization and possibly increasing the cost. That is:

$$V_N^{uc} = V_f(x) \leq V_N^0, \quad \forall \mathcal{X}_N \supseteq \mathbb{X}_f$$

From proposition 2.18 in [7] we obtain that $V_j^0(x) \leq V_f(x) \quad \forall x \in \mathbb{X}_f, \forall j \in \mathbb{N}$. By the latter and the former fact we deduce that $V_N^0(x) = V_f(x)$:

$$\begin{aligned} V_N^{uc} = V_N^0(x) = V_f(x) = V_\infty^{uc}(x), &\qquad \forall x \in \mathbb{X}_f \\ \kappa_N(x) = \kappa_\infty^{uc}(x) = Kx, &\qquad \forall x \in \mathbb{X}_f \end{aligned}$$

The former implies the latter since they have the same optimizers. The latter holds $\forall x \in \mathbb{X}_f$ by uniqueness of the solution. In conclusion, this proves that $\mathbb{X}_f$ is positive control invariant for $x^+ = Ax + B\kappa_N(x)$ ■

B. Asymptotic stability under MPC

Now follows the proof of theorem 2.24 from [7] to prove asymptotic stability of the origin when closing the loop using MPC. In particular, it states that if assumptions 2.2, 2.3, 2.14, and 2.17 (i.e., from [7]) are satisfied then the origin is asymptotically stable in the region of attraction $\mathcal{X}_N$ for $x^+ = f(x, \kappa_N(x))$, where $\mathcal{X}_N$:

$$\mathcal{X}_N = \{x_0 \in \mathbb{R}^{n_x} \mid \mathcal{U}_N(x_0) \neq \emptyset\} \tag{21}$$

$$\begin{aligned} \mathcal{U}_N(x_0) = \{&\mathbf{u}_N \in \mathbb{R}^{n_u N} \mid x(k) = \phi(k; x_0, \mathbf{u}_k), \\ &(x(k), u(k)) \in \mathbb{Z}, \forall k \in \mathbb{N}, x(N) \in \mathbb{X}_f\} \subseteq \mathbb{U}^N \end{aligned} \tag{22}$$

Now follows the verification of the stated assumptions.

Assumption 2.2 ([7]): *(i) The function $f : \mathbb{Z} \to \mathbb{X}$ is continuous as it doesn't include abrupt changes of value (i.e., jumps). Its linearization preserves continuity. (ii) We recall from section II that $l(x,u) : \mathbb{Z} \to \mathbb{R}^+$ is quadratic and hence continuous and that $Q \succ 0, R \succ 0$ implies $l(x,u) \succ 0$ and $l(0,0) = 0$. (iii) Equivalently, $P \succ 0$ implies $V_f(x) \succ 0$ and $V_f(0) = 0$. In addition, $V_f(x)$ is quadratic in x hence continuous. This verifies Assumption 2.2.*

Assumption 2.3 ([7]): *(i) The sets $\mathbb{X}$ and $\mathbb{U}$ are closed and bounded as defined in equation 14. In fact, by the Heine-Borel theorem, any closed and bounded set in $\mathbb{R}^n$ is compact. From the previous facts we deduce that $\mathbb{X}$ and $\mathbb{U}$ are compact, and $\mathbb{Z}$ is closed. (ii) Equivalently, $\mathbb{X}_f \subseteq \mathbb{X}$ is closed and bounded hence compact. (iii) By equation 14 $\mathbb{U}$ is compact and $0 \in$ int($\mathbb{U}$). $\mathbb{X}_f$ is an ellipsoidal set around the origin hence $0 \in$ int($\mathbb{X}_f$) and since $\mathbb{X}_f \subseteq \mathbb{X}$ then $0 \in$ int($\mathbb{X}$). This verifies assumption 2.3.*

The above assumptions guarantee continuity of the cost function in $\mathbb{Z}$, compactness of $\mathcal{U}_N$, and most importantly existence of a solution to $\mathbb{P}_N$ (by proposition 2.4 in [7]). The following is a basic stability assumption in the terminal set.The last assumption verifies what is called *weak* controllability.

Assumption 2.14 ([7]): *(a) Using the notation defined in section II we must show that $V_f(A_Kx) \leq V_f(x) - l(x,u)\ \forall x \in \mathbb{X}_f$. Observe that $V_f(A_Kx) = \frac{1}{2}x^TA_K^TPA_Kx$. Assuming the Lyapunov equation is solvable $V_f(A_Kx) = \frac{1}{2}x^TPx - \frac{1}{2}x^TQ_Kx$ and by definition $x^TQ_Kx = x^T(Q + K^TRK)x = x^TQx + x^TK^TRKx$. Due to the feedback law $u = -Kx$ we*

have that $x^T Q_K x = x^T Q x + u^T R u = l(x,u)$. Hence we can substitute this into:

$$V_f(A_K x) = \frac{1}{2}x^T P x - \frac{1}{2}l(x,u) \leq V_f(x) - \frac{1}{2}l(x,u)$$

From Lemma 1 it follows that $\kappa_N(x) = Kx\ \forall x \in \mathbb{X}_f$ and that $\mathbb{X}_f$ is positive invariant under the MPC control law. By the facts stated above we conclude that assumption 2.14(a) holds. (b) Now we prove lower and upper boundedness by a class $\mathcal{K}_\infty$ of (i) $l(x,u)$ and (ii) $V_f(x)$ respectively. (i) It is easy to see that $\frac{1}{2}x^T Q x + \frac{1}{2}u^T R u \geq \frac{1}{2}x^T Q x \geq \frac{1}{2}\lambda_{min}(Q)|x|^2$. $\frac{1}{2}\lambda_{min}(Q)|x|^2 \in \mathcal{K}_\infty$ since it is continuous, zero at zero, strictly increasing and unbounded. This inequality always holds in the domain of reals, hence also for $x \in \mathcal{X}_N$ and $(x,u) \in \mathbb{Z}$. (ii) $V_f(x) = \frac{1}{2}x^T P x \leq \frac{1}{2}\lambda_{max}(P)|x|^2$. By the same reasoning as before, the upper bound is in the class $\mathcal{K}_\infty$.

Assumption 2.17 [7]: *By the proof in Lemma 1 $V_N^0(x) = V_f(x) \leq \frac{1}{2}\lambda_{max}(P)|x|^2$. The latter is a class $\mathcal{K}_\infty$ function since it's continuous, zero at zero, strictly increasing, and unbounded. Furthermore, it holds $\forall x \in \mathbb{X}$ hence also $\forall x \in \mathcal{X}_N$ since $\mathcal{X}_N \subseteq \mathbb{X}$. This verifies assumption 2.17.*

In conclusion, we have verified all the assumptions of Theorem 2.24 from [7] and we can therefore conclude that the origin is asymptotically stable in the region of attraction $\mathcal{X}_N$ for $x^+ = f(x, \kappa_N(x))$, using our MPC design. Note that, as mentioned in [7] (see page 356), if the stability assumptions hold for $\mathbb{X}_f$, they hold for $\mathbb{X}_f'$ as well, albeit for a different region of attraction $\mathcal{X}_n'$.

IV. Numerical Simulations

In this section, we run several numerical simulations in which we compare our state and output feedback MPC designs with the LQR design employed in reference [4].

A. Simulation Procedure

In order to numerically simulate the behavior of the AC45, a prediction model is needed. The system matrices are utilized to create the prediction model matrices T and S. These matrices capture the system's evolution from both the initial state and input sequences. each row in the prediction matrix T represents the effect of the initial condition at each time step, whilst the matrix S incorporates the effects of the input sequences on the evolution of the state.

$$T = \begin{bmatrix} I \\ \Psi \\ \Psi^2 \\ \vdots \\ \Psi^N \end{bmatrix},\ S = \begin{bmatrix} 0 & 0 & \cdots & 0 \\ \Gamma & 0 & \ddots & \vdots \\ \Psi\Gamma & \Gamma & \ddots & 0 \\ \vdots & \ddots & \ddots & 0 \\ \Psi^{N-1}\Gamma & \Psi^{N-2}\Gamma & \cdots & \Gamma \end{bmatrix} \tag{23}$$

such that $\mathbf{x}_{N+1} = Tx_0 + S\mathbf{u}_N$.

These matrices are then used to construct the cost function, by defining:

$$\bar{Q} = \begin{bmatrix} I_N \otimes Q & 0 \\ 0 & P \end{bmatrix},\ \bar{R} = I_N \otimes R \tag{24}$$

$$H = S^T \bar{Q} S + \bar{R} \tag{25}$$

$$\begin{aligned} \mu_{x_0} &= S^T \bar{Q} T,\ \mu_{x_{ref}} = -S^T \bar{Q}(\mathbf{1}_{N+1} \otimes I_{n_x}) \\ \mu_{u_{ref}} &= -\bar{R}(\mathbf{1}_N \otimes I_{n_u}),\ \bar{\mu} = \begin{bmatrix} \mu_{x_0} & \mu_{x_{ref}} & \mu_{u_{ref}} \end{bmatrix} \end{aligned} \tag{26}$$

where Q and R are the weight matrices defined in Section II. Let $\rho^T = \begin{bmatrix} x_0^T & x_{ref}^T & u_{ref}^T \end{bmatrix}$ and define $\tilde{\mathbf{F}} = blkdiag(\mathbf{F}, \ldots, \mathbf{F})$, $\tilde{\mathbf{E}} = blkdiag(\mathbf{E}, \ldots, \mathbf{E})$, and $\tilde{\mathbf{e}} = \mathbf{1}_{N\times 1} \otimes \mathbf{e}$. Then we can compactly write the QCQP:

$$\begin{aligned} V_N(x, \mathbf{u}_N) &= \frac{1}{2}\mathbf{u}_N^T H \mathbf{u}_N + \bar{\mu}^T \rho^T \mathbf{u}_N \\ \text{s.t.}\quad & \tilde{\mathbf{F}} T x_0 + (\tilde{\mathbf{F}} S + \tilde{\mathbf{E}})\mathbf{u}_N \leq \tilde{\mathbf{e}} \\ & (x_N - x_{ref})^T P (x_N - x_{ref}) \leq 1 \\ & x_0 = x(k) \end{aligned} \tag{27}$$

where x_N is obtained from the last n_x rows of S and T.

In order to solve the optimization problem we used the Matlab package YALMIP. The choice to use this package was based mainly on the ease of use and the ability to easily specify the desired optimization algorithm.

B. State Feedback with different horizons

Figure 3 displays the system response for several values of N. The reference output is chosen as $y_{ref} = \begin{bmatrix} 0.3 & 0 \end{bmatrix}^T$ and the optimization flag is verified to be 0 at all times. It is clear that for all values of N the output converges to the desired reference. The time required to correct the ride height error is approximately 1 second, which is similar to the result obtained by [4]. On observing the pitch angle, there appears to be a trade-off between the settling time and the overshoot. Using $N = 10$ leads to a maximum angle that is roughly twice as large as when using $N = 20$. It should be kept in mind that it is not desirable for the ship to change pitch too quickly, as this leads to discomfort and is not realistic for humans to replicate in a racing scenario.

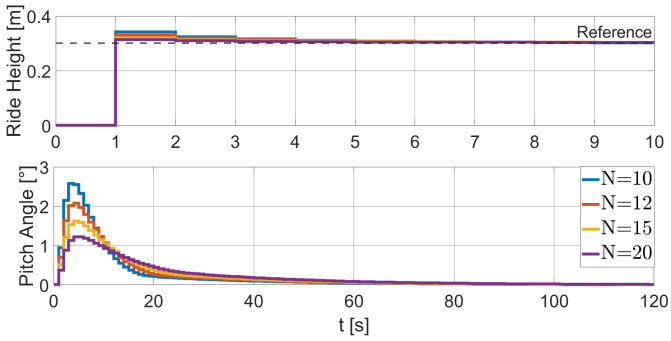

Fig. 3. System outputs using state feedback with a ride height reference of 0.3 meters and 4 prediction horizons

When investigating the inputs shown in figure 4 we see that there are initial changes in the rudder and daggerboard angle which decrease as the error between the states and reference grows smaller. Note that initially the rudder angle is positive, whilst the daggerboard rake angle is negative.

This indicates that both the stern and the CM are pushed up. Further on, the angles are both positive, meaning the CM is pushed down to stabilize at reference height. Furthermore, the pitch angle converges slowly from a slight 'bow-down' position to 0° pitch. In general, the control action is relatively aggressive. However, with a longer horizon the action becomes less aggressive, making the case strong to choose $N = 20$.

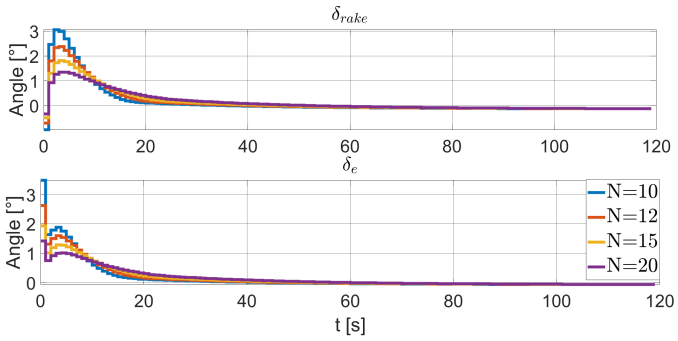

Fig. 4. System inputs using state feedback with a ride height reference of 0.3 meters and 4 prediction horizons

Table II shows the difference in the YALMIP time and the solver time for two horizons. As expected, the solver time for $N = 10$ is much faster than for $N = 20$. More precisely, it is approximately four times faster, which may indicate a quadratic relation between prediction horizon and solver time. Furthermore, it must be noted that the solver time using $N = 20$ is still 0.1 seconds shorter than the sampling time.

Horizon	**YALMIP** t (sec)	**Solver** t (sec)
$N = 10$	0.2	0.09
$N = 20$	0.23	0.4

TABLE II
COMPARISON OF OPTIMIZATION TIMES FOR THE SHORT AND LONG HORIZON CASE

C. LQR vs. MPC - State Feedback

The LQR controller design is compared to the MPC design using two different set of weights. The first set of weights is is obtained from the error dynamics weights in reference [4]. The second set of weights corresponds to the weights used in the MPC problem formulation.

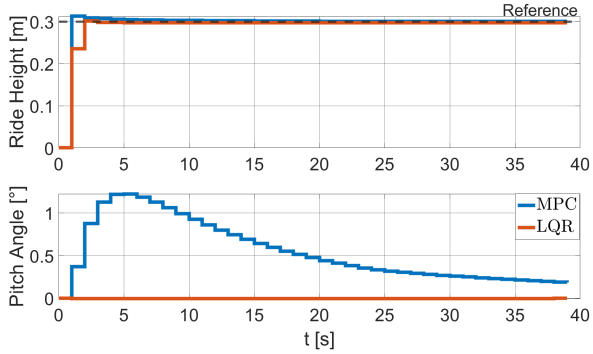

Fig. 5. MPC vs LQR with $Q = diag(0, 0, 0, 0.5, 0.005)$ and $R = I_{n_u}$

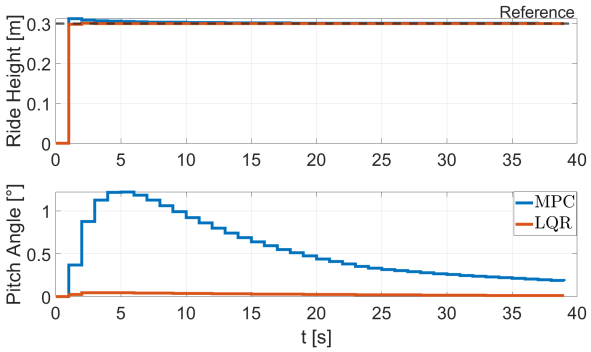

Fig. 6. MPC vs LQR with weight used in the MPC formulation

It is observed that in both cases, both the LQR and MPC controller succeed in quickly tracking the desired ride height. Furthermore, it is apparent that the MPC controller allows for changes in the pitch of the vessel over time, while the LQR controller does not signficantly deviate the pitch. However, it is important to note that these simulations are performed without disturbances, meaning that the effects of waves, currents and changing wind conditions are not taken into consideration, while dealing with these factors is where the strength of the MPC controller is expected to lie. Furthermore, the LQR has an agressive, underdamped response which might not be ideal in real applications.

D. Output Feedback - Noise & Disturbance

In conclusion, we show the results for reference tracking with constant disturbances and random noise, the more realistic case. The prediction horizon is $N = 20$ and $y_{ref} = \begin{bmatrix} 0.3 & 0 \end{bmatrix}^T$. Furthermore, the actual and estimated states have different initial conditions as $x_0 = \begin{bmatrix} 0 & 0 & 0 & -0.1 & 0 \end{bmatrix}^T$ and $\hat{x}_0 = \begin{bmatrix} 0 & 0.05 & 0 & 0 & -0.05 \end{bmatrix}^T$. The optimization flag is verified to be 0 at all times and the reported performance is YALMIP t 0.51 sec and Solver t 0.29 sec.

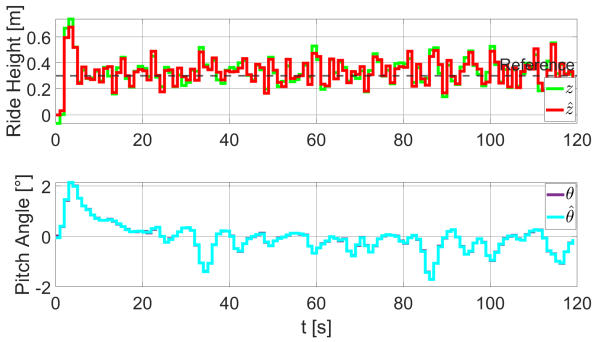

Fig. 7. System outputs using output feedback with constant disturbance and noise; ride height reference of 0.3 meters and prediction horizon N=20

The MPC law stabilizes the outputs within a variance band around the reference; shown in figure 7 and for multiple experiments in figure 8. We can never achieve offset free stabilization due to the addition of the noise. In comparison to the state feedback case, the initial overshoot for both outputs is significantly higher. Notably, the state falls outside of the constraints due to unmodelled additive noise.

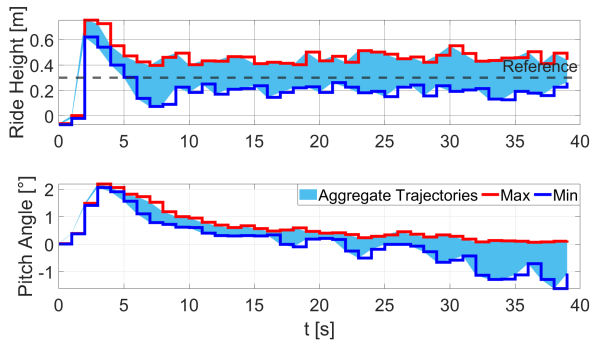

Fig. 8. Trajectories of z and θ during 10 experiments highlighting the minimum, maximum, and the aggregate of the other possible trajectories

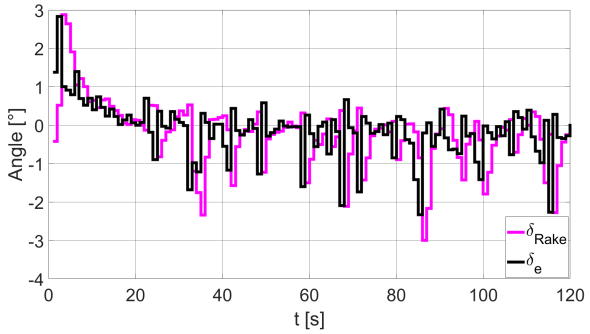

Fig. 9. System inputs using output feedback with constant disturbance and noise; ride height reference of 0.3 meters and prediction horizon N=20

The pitch starts again in a 'bow-down' position but has a tendency to react with 'bow-up' movements (negative yaw). The latter is visible in the seemingly larger negative action of the daggerboard in figure 9. In general, the control action is quite aggressive.

In conclusion, it can be seen that the disturbance estimations do not converge to 0 due to noise (figure 10). However, the estimation error stays within a variance around 0, which is relatively (w.r.t. the disturbance) large, especially for d_2.

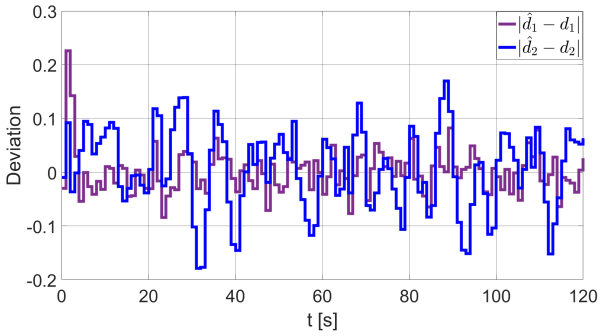

Fig. 10. Deviation of actual disturbance from estimated disturbance

V. Conclusion

In this paper, we have used linear MPC for the longitudinal stabilization of an AC45 hydrofoiling catamaran. First, we have transformed the continuous-time model to a discrete-time model with additive disturbances. Subsequently, we have provided a structured stability proof for state-feedback MPC using an ellipsoid terminal set. Lastly, numerical simulations have shown the performance of the design at hand.

A linear MPC controller for longitudinal stabilization of an AC45 shows promising results, even in heavily disturbed conditions. The computational time is good but could be improved by using better CPUs and lower-level coding languages. On a more critical note, it would have been desirable to use a higher sampling frequency. However, decreasing the inter-sampling time has led to infeasible optimization problems. Our hypothesis is that the solver encountered problems due to small values in the Hessian, especially found in higher powers of Ψ. This could be resolved by using a non-convex optimization algorithm (e.g., quasi-newton), although this incites a higher computational time. This is doubly troubling, as it means the time needed to compute the solution to the optimization problem is longer while the time in which the problem needs to be solved becomes shorter. Furthermore, we must note that the control action is relatively aggressive, an aspect that might be improved in a subsequent design through rate of change constraints.

References

[1] A. F. Molland and S. R. Turnock, "Chapter 4 - hydrofoils," in *Marine Rudders, Hydrofoils and Control Surfaces (Second Edition)*, second edition ed., A. F. Molland and S. R. Turnock, Eds. Oxford: Butterworth-Heinemann, 2022, pp. 57–89. [Online]. Available: https://www.sciencedirect.com/science/article/pii/B9780128243787000056

[2] A. Cup, *AC75 Class Rules v2.0*, 2022.

[3] R. Gladwell. (2023) America's cup: Look, ma - no hands! flying the ac40 explained. [Online]. Available: https://www.sail-world.com/news/266143/Americas-Cup-Look-Ma-No-hands

[4] R. Bencatel, S. Keerthivarman, I. Kolmanovsky, and A. Girard, "Full state feedback foiling control for america's cup catamarans," *IEEE Transactions on Control Systems Technology*, vol. PP, pp. 1–17, 01 2020.

[5] Y. Wang, L. Bai, and S. Liu, "Nonlinear control of hydrofoil catamaran course in three dof," in *2014 IEEE Conference and Expo Transportation Electrification Asia-Pacific (ITEC Asia-Pacific)*, 2014, pp. 1–6.

[6] J. van Schuppen, *Control and System Theory of Discrete-Time Stochastic Systems*, ser. Communications and Control Engineering. Springer, 2021, no. 923.

[7] J. Rawlings and D. Mayne, *Model Predictive Control: Theory and Design*. Nob Hill Publishing, 2008.

[8] G. Pannocchia and J. B. Rawlings, "Disturbance models for offset-free model-predictive control," *Aiche Journal*, vol. 49, pp. 426–437, 2003. [Online]. Available: https://api.semanticscholar.org/CorpusID:10867777

[9] G. Besana, "Computational methods for hydrofoil design - a composite analysis using panel code and rans," Ph.D. dissertation, 01 2015.

[10] Z. Ni, M. Dhanak, and T. chow Su, "Performance of a hydrofoil operating close to a free surface over a range of angles of attack," *International Journal of Naval Architecture and Ocean Engineering*, vol. 13, pp. 1–11, 2021. [Online]. Available: https://www.sciencedirect.com/science/article/pii/S2092678220300509